Metrol. Meas. Syst., Vol. 32 (2025) No. 2, pp. 1–14
DOI: 10.24425/mms.2023.154667

PAN POLSKA AKADEMIA NAUK

METROLOGY AND MEASUREMENT SYSTEMS
Index 330930, ISSN 0860-8229
www.metrology.wat.edu.pl

M&MS

ALGORITHM FOR ESTIMATING BALLISTIC OBJECT TRAJECTORIES USING AN ELECTRO-OPTICAL TRACKING SYSTEM

Piotr Smagowski[1)], Piotr Kaniewski[2)]

1) Wroclaw University of Technology, Faculty of Electronics, Photonics and Microsystems, ul. Janiszewskiego 11-17, 50-372 Wrocław, Poland
2) Military University of Technology, Faculty of Electronics, Gen. S. Kaliskiego 2, 00-908 Warsaw, Poland (✉ *piotr.kaniewski@wat.edu.pl*)

Abstract

This paper presents an estimation algorithm designed for tracking aerial ballistic objects using measurements from an electro-optical tracking system. Building upon our previous research, which focused on estimating the trajectory and flight parameters of an unguided short-range ballistic missile with motion constrained to two dimensions, this study introduces a more advanced and practical solution. The new approach uses a flight dynamics model formulated in a three-dimensional coordinate system. Unlike the previously developed algorithm, the one described in this paper accurately determines the object's location within a geographically oriented horizontal reference frame. It also eliminates the need for prior knowledge of the shooting direction, which would be challenging to establish in practice, and more realistically models the influence of wind on the object's motion in three dimensions. The paper includes the mathematical model of the tracking system, the extended Kalman filter used for estimating the ballistic object's position and other flight parameters as well as simulation results for the proposed system.

Keywords: electro-optical tracking system, ballistic object, extended Kalman filter, aerial target tracking.

1. Introduction

The motivation for this work arose during the development of algorithms for unguided missile trajectory estimation using measurements from an *Electro-Optical Tracking System* (EOTS) [1]. EOTS is a highly accurate system that can be used to assess missile characteristics, such as aerial object positions, flight parameters, and miss distance during rocket weapon testing. In Poland, such a system was installed and operated at the premises of the *Military Institute of Armament Technology* (MIAT), Zielonka, where the first author, while a member of the MIAT staff, extensively used it in various real-world tests of ballistic objects. This experience inspired the authors to develop more advanced and versatile localization algorithms to replace the previously used methods, which were based on straightforward geometric computations and had several limitations. When starting the research, it was assumed that the Kalman filter would allow for more accurate estimation of the flight parameters of the ballistic object under consideration.

Article history: received February 12, 2025; revised April 2, 2025; accepted April 9, 2025; available online May 16, 2025.

The research presented in this paper builds upon our previous work, which focused on estimating the trajectory and flight parameters of an unguided short-range ballistic missile, with its motion constrained to two dimensions only [2]. The object motion in that study was restricted to *three degrees of freedom* (3-DOF), simplifying the system's model but limiting its practical application. This paper introduces a more advanced and practical solution, using a flight dynamics model formulated in a three-dimensional coordinate system and accounting for the object's movement in *six degrees of freedom* (6-DOF), including both linear and rotational components in three dimensions. Unlike the previous algorithm, the one presented here accurately determines the object's location within a geographically oriented horizontal frame of reference, does not require prior knowledge of the shooting direction (which is difficult to establish in practice), and more realistically models the influence of winds on the object's motion in three dimensions.

The structure of the paper is as follows. Section 2 describes the mathematical model, and the estimation algorithm proposed for the electro-optical tracking system. Section 3 presents the results of the performed tests, while Section 4 offers a discussion of the findings.

The main contribution of this paper is the development of a practical algorithm for estimating the trajectories and flight parameters of aerial ballistic objects using the six-degrees-of-freedom equations of ballistic object motion for an electro-optical tracking system. Additionally, the paper presents simulation results that assess the expected accuracy of EOTS with the proposed tracking algorithm.

2. Materials and methods

Radar and optical observation and tracking systems [3–11], when estimating the position and other flight parameters of observed objects, often employ *Extended Kalman Filters* (EKFs) [8–11]. EKF belongs to the model-based category of estimation algorithms and requires the formulation of both the dynamics and observation models of the tracking system [12]. It is particularly suitable for systems with non-linear dynamics and/or non-linear observation models, which applies to the problem at hand.

The dynamics model in tracking systems typically includes the equations of object motion. Depending on the object type and the adopted simplifying assumptions, this model can be either linear or non-linear [9, 13]. In the case of ballistic objects, which are the focus of this research, aerodynamics models are used to formulate the dynamics. These models are typically represented by systems of non-linear differential equations [13–16].

The observation model defines the relationship between the object's position coordinates and the measurements made by the system. In the case of EOTS, the measurements consist of the azimuth and elevation angles from ground-based electro-optical tracking stations (cinetheodolites) to the observed object [1], making this relationship inherently non-linear.

EKFs address non-linearities in one or both models through linearization, which involves calculating Jacobian matrices for the non-linear functions in the models [12]. While this slightly increases the algorithm's complexity compared to the linear Kalman filter, the added complexity is typically manageable with the modern computing power available in radar and optical tracking systems. Therefore, we have chosen to use the EKF in the system considered here.

The following subsections of the paper describe the estimation framework, with a focus on its key components: the dynamics and measurement models, as well as the filtering algorithm.

2.1. Dynamics model

In the system under consideration, the motion of a ballistic object is modelled using 6-DOF differential equations of motion. A comprehensive description of such motion, considering both translational and rotational movements, is presented in [14, 15]. In this work, we adapted the dynamics model to match a typical object used in experiments conducted at MIAT, *i.e.* the aerial target imitator ICP-89, a small, short-range, unguided rocket [17]. This object does not contain a warhead but features a tracer with burning material to enhance visibility from the EOTS cinetheodolites. The thrust force generated by its solid propellant lasts for only about 0.7 seconds, after which the rocket moves freely without propulsion for the remainder of its flight.

Figure 1 illustrates the aerial object in a right-handed, three-dimensional frame of reference ($EXYZ$), showing the forces acting on it during various flight phases, along with key variables defining its motion. In this figure, O represents the centre of mass (m) of the object, $\mathbf{F_l}$ is the lift force, $\mathbf{F_d}$ is the drag force, $\mathbf{F_g}$ is the gravitational force, and $\mathbf{F_t}$ is the thrust force. The instantaneous position of the object is described by its coordinates x, y, and h. Other important variables include: $\mathbf{v}$ – the velocity vector relative to the atmosphere, γ – the angle between the velocity vector and the local horizontal plane (EXY), χ – the angle between the X-axis and the velocity vector projected onto the horizontal plane (EXY), α – the angle of attack (the angle between the reference line of the body, *i.e.*, its longitudinal axis and the relative velocity vector), and ϵ_0 – the angle between the longitudinal axis and the thrust force vector.

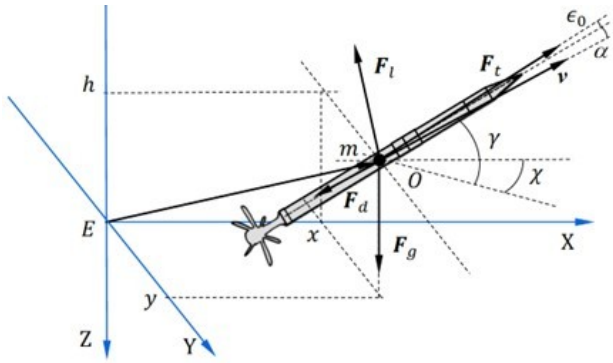

Fig. 1. Aerial target with forces acting on it in a three-dimensional frame of reference.

The general 6-DOF equations of motion for a ballistic object, neglecting disturbances caused by winds, are given as follows [14]:

$$\dot{x} = v\cos\gamma\cos\chi, \tag{1}$$

$$\dot{y} = v\cos\gamma\sin\chi, \tag{2}$$

$$\dot{h} = v\sin\gamma, \tag{3}$$

$$\dot{v} = \frac{1}{m}\left[F_t\cos(\alpha+\epsilon_0) - F_d - F_g\sin\gamma\right], \tag{4}$$

$$\dot{\gamma} = \frac{1}{mv}\left[F_t\sin(\alpha+\epsilon_0) + F_l\right]\cos\mu - \frac{1}{mv}F_g\cos\gamma, \tag{5}$$

$$\dot{\chi} = \frac{1}{mv\cos\gamma}\left[F_t\cos(\alpha+\epsilon_0) + F_l\right]\sin\mu, \tag{6}$$

$$\dot{F_g} = -C_f F_t. \tag{7}$$

Additional variables not previously explained include: v – the magnitude of the velocity vector, μ – the roll angle, and C_f – the fuel consumption coefficient.

Given the stable, unguided flight of the object, a simplified mathematical model of its movement can be applied under the following assumptions:

- The object's flight is modelled after the propellant has completed its working phase, and the EOTS is tracking the imitator when the thrust force becomes zero.
- The lift force can be neglected due to the object's axial symmetry and absence of large aerofoils. Thus, the forces considered in the model include only drag, gravity, and wind forces.
- The atmospheric density significantly varies with altitude and must be incorporated into the dynamics model.
- The object's mass decreases slowly over time, not due to fuel consumption (as combustion has ceased in this phase of flight), but due to the tracer burnout. Therefore, instead of using (7), the following formula applies, where C_m is the tracer burnout coefficient, describing the mass loss over time:

$$\dot{m} = -C_m. \tag{8}$$

The gravity and drag forces in (4) and (5) can be calculated as follows [14]:

$$F_g = mg, \tag{9}$$

$$F_d = \frac{1}{2} C_d S \rho(h) v^2, \tag{10}$$

where: g is the gravitational acceleration, C_d is the drag coefficient, S is the drag characteristic surface area, and $\rho(h)$ is the air density at altitude h. For altitudes up to 11 kilometres, the following relationship holds, with ρ_0 representing the sea-level air density under normal weather conditions [18]:

$$\rho(h) = \rho_0 \left(1 - \frac{h}{44300}\right)^{4.256}. \tag{11}$$

In practice, unpredictable wind influences will affect the ideal ballistic trajectory described by (1)–(7). We model the wind velocity as an additional stochastic process with three components w_x, w_y, and w_h along the axes of the $EXYZ$ frame of reference. These components are modelled as integrated Gaussian white noises with power spectral densities S_{wx}, S_{wy}, and S_{wh}. Therefore, the following differential equations hold:

$$\dot{w}_x = u_{wx}, \tag{12}$$

$$\dot{w}_y = u_{wy}, \tag{13}$$

$$\dot{w}_h = u_{wh}. \tag{14}$$

The disturbances caused by the wind affect not only the position (1)–(3) but also influence the equations for velocity and attitude angles (4)–(6). By applying the previously mentioned simplifications to (1)–(6), substituting the right-hand sides of formulas (9)–(11) for the respective variables and incorporating the wind velocities into the motion equations, we obtain the following continuous dynamics model for the ballistic object [1].

The equation (15) closely follows the standard form required for further development of the extended Kalman filter [12]:

$$\begin{bmatrix} \dot{x} \\ \dot{y} \\ \dot{h} \\ \dot{v} \\ \dot{\gamma} \\ \dot{\chi} \\ \dot{m} \\ \dot{w}_x \\ \dot{w}_y \\ \dot{w}_h \end{bmatrix} = \begin{bmatrix} v\cos\gamma\cos\chi + w_x \\ v\cos\gamma\cos\chi + w_y \\ v\sin\gamma + w_h \\ -\dfrac{1}{2m}C_d S v^2 \rho_0 \left(1 - \dfrac{h}{44300}\right)^{4.256} - g\sin\gamma \\ -\dfrac{g}{v}\cos\gamma \\ 0 \\ -C_m \\ 0 \\ 0 \\ 0 \end{bmatrix} \begin{bmatrix} 0 & 0 & 0 \\ 0 & 0 & 0 \\ 0 & 0 & 0 \\ -\dfrac{\cos\gamma\cos\chi}{v} & -\dfrac{\cos\gamma\sin\chi}{v} & -\dfrac{\sin\gamma}{v} \\ \dfrac{\sin\gamma\cos\chi}{v} & \dfrac{\sin\gamma\sin\chi}{v} & -\dfrac{\cos\gamma}{v} \\ \dfrac{\sin\chi}{v\cos\gamma} & -\dfrac{\cos\chi}{v\cos\gamma} & 0 \\ 0 & 0 & 0 \\ 1 & 0 & 0 \\ 0 & 1 & 0 \\ 0 & 0 & 1 \end{bmatrix} \cdot \begin{bmatrix} u_{wx} \\ u_{wy} \\ u_{wh} \end{bmatrix}. \tag{15}$$

$$\dot{\mathbf{x}}(t) = \mathbf{f}[\mathbf{x}(t)] + \mathbf{G}(t)\,\mathbf{u}(t), \tag{16}$$

where: $\mathbf{f}(\cdot)$ is a nonlinear function, $\mathbf{x}$ is the state vector, $\mathbf{G}$ is the disturbance input matrix, and $\mathbf{u}$ is the vector of disturbances.

2.2. Observation model

A typical deployment of EOTS stations (cinetheodolites) in the three-dimensional Cartesian reference frame $EXYZ$ is shown in Fig. 2. The cinetheodolites labelled as S_1 and S_2 are located at coordinates (x_1, y_1, z_1) and (x_2, y_2, z_2), respectively. Their positions are accurately determined prior to the shooting tests. During operation, these stations provide a synchronized stream of measurements for the azimuth angles α_1 and α_2 and the elevation angles λ_1 and λ_2.

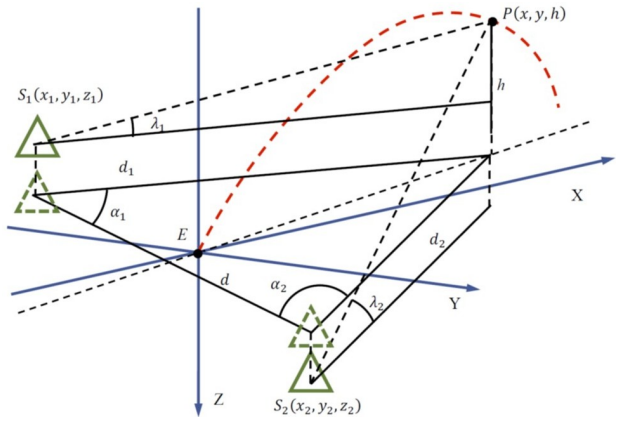

Fig. 2. Geometrical relationships and measurements performed in EOTS.

The observation model relates the state vector $\mathbf{x}$ to the measurement vector $\mathbf{z}$. In the system under consideration, the relationship between the object's position coordinates (x, y, h) and the measured angles α_1, α_2, λ_1, and λ_2 is nonlinear. Therefore, before designing the extended Kalman filter, the observation model is cast in the standard form:

$$\mathbf{z}(k) = \mathbf{h}[\mathbf{x}(k)] + \mathbf{v}(k), \tag{17}$$

where: $\mathbf{h}(\cdot)$ is a nonlinear function, $\mathbf{z}$ is the measurement vector, $\mathbf{x}$ is the state vector, and $\mathbf{v}$ is the measurement error vector.

Directly inserting the measured angles α_1, α_2, λ_1, and λ_2 into the measurement vector is not possible. This difficulty arises because the equations that relate these angles to the ballistic object's coordinates (x, y, h) and the cinetheodolites' positions (x_1, y_1, z_1) and (x_2, y_2, z_2) form an entangled system that does not match the structure of (18).

To resolve this issue, we first define a primary measurement vector $\mathbf{z}'$:

$$\mathbf{z}' = [\alpha_1 \, \alpha_2 \, \lambda_1 \, \lambda_2 \,]^T \tag{18}$$

and then transform it using an appropriately chosen function $\mathbf{t}(\cdot)$ so that the transformed measurement vector $\mathbf{z} = \mathbf{t}(\mathbf{z}')$ leads to a measurement model of the form (18), with the left-hand side containing only measurement-related variables and the right-hand side involving only the state vector components.

To establish the transformation function $\mathbf{t}(\cdot)$, we use the law of sines and other trigonometric relationships valid in the considered system:

$$\frac{\sqrt{(x-x_2)^2+(y-y_2)^2}}{\sin\alpha_1} = \frac{\sqrt{(x_1-x_2)^2+(y_1-y_2)^2}}{\sin(\alpha_1+\alpha_2)}, \tag{19}$$

$$\frac{\sqrt{(x-x_1)^2+(y-y_1)^2}}{\sin\alpha_2} = \frac{\sqrt{(x_1-x_2)^2+(y_1-y_2)^2}}{\sin(\alpha_1+\alpha_2)}, \tag{20}$$

$$h + z_1 = \sqrt{(x-x_1)^2+(y-y_1)^2}\tan\lambda_1, \tag{21}$$

$$h + z_2 = \sqrt{(x-x_2)^2+(y-y_2)^2}\tan\lambda_2. \tag{22}$$

Assuming that the measured angles are not exact but are subject to errors $v_{\alpha 1}$, $v_{\alpha 2}$, $v_{\lambda 1}$, and $v_{\lambda 2}$, the transformation leads to a measurement model that can be expressed as:

$$\begin{bmatrix} \dfrac{\sin\alpha_1}{\sin(\alpha_1+\alpha_2)} \\ \dfrac{\sin\alpha_2}{\sin(\alpha_1+\alpha_2)} \\ \tan\lambda_1 \\ \tan\lambda_2 \end{bmatrix} = \begin{bmatrix} \sqrt{\dfrac{(x-x_2)^2+(y-y_2)^2}{(x_1-x_2)^2+(y_1-y_2)^2}} \\ \sqrt{\dfrac{(x-x_1)^2+(y-y_1)^2}{(x_1-x_2)^2+(y_1-y_2)^2}} \\ \dfrac{h+z_1}{\sqrt{(x-x_1)^2+(y-y_1)^2}} \\ \dfrac{h+z_2}{\sqrt{(x-x_2)^2+(y-y_2)^2}} \end{bmatrix} + \begin{bmatrix} v_1 \\ v_2 \\ v_3 \\ v_4 \end{bmatrix}. \tag{23}$$

In this formulation, the left-hand side represents the transformed measurements (*i.e.*, the output of the transformation function $\mathbf{t}(\mathbf{z}')$, while the right-hand side comprises functions of the state variables and a measurement error vector $\mathbf{v} = [v_1 \, v_2 \, v_3 \, v_4]^T$.

Finally, the measurement error vector $\mathbf{v}$ is related to the primary measurement errors $\mathbf{v}' = [v_{\alpha 1} \, v_{\alpha 2} \, v_{\lambda 1} \, v_{\lambda 2}]^T$ via the Jacobian matrix $\mathbf{T} = \dfrac{\partial \mathbf{t}(\mathbf{z}')}{\partial \mathbf{z}'}$ of the transformation, so that $\mathbf{v} = \mathbf{T}\mathbf{v}'$.

This approach ensures that the measurement model is expressed in a form compatible with the extended Kalman filter framework.

Metrol. Meas. Syst., Vol. 32 (2025), No. 2, pp. 1–14
DOI: 10.24425/mms.2023.154667

2.3. Estimation algorithms

The primary estimation algorithm used in this research is the *extended Kalman filter* (EKF). For comparison, simpler *ordinary least squares* (OLS) and *weighted least squares* (WLS) algorithms [19] have also been implemented and tested. The EKF employs the previously described dynamics and observation models, and its block diagram is shown in Fig. 3.

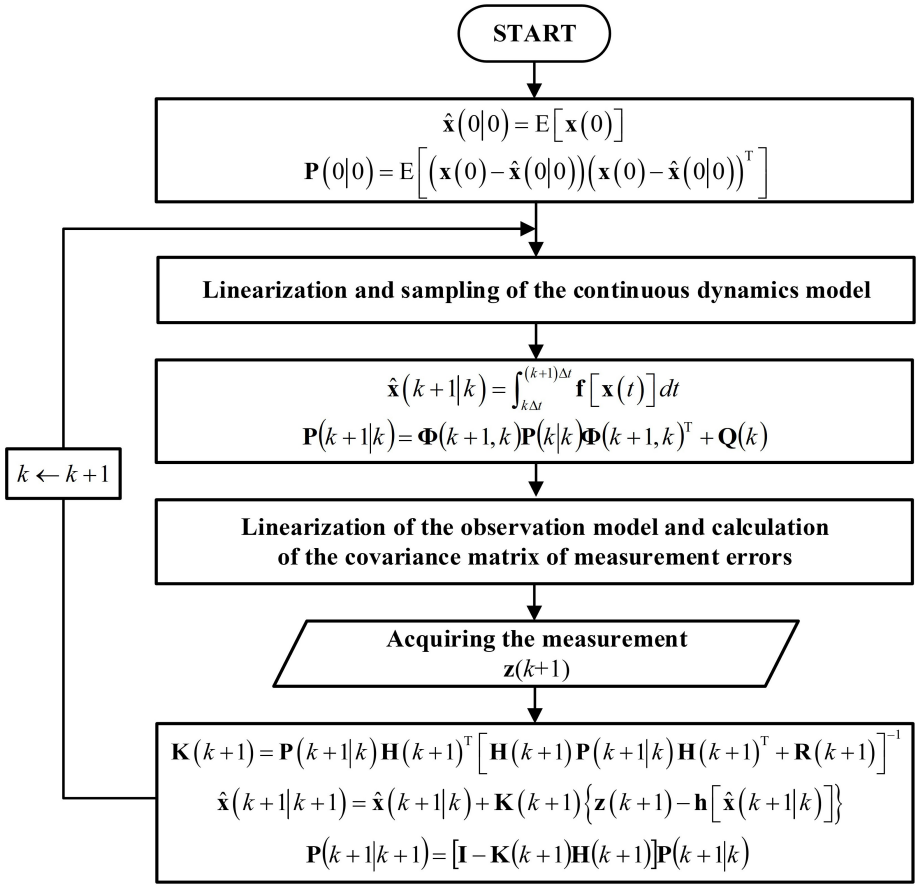

Fig. 3. Block diagram of the EKF algorithm.

After initialization, which involves defining the initial estimated state vector $\hat{x}\,(0\,|\,0)$ and the initial covariance matrix of filtering errors $\mathbf{P}\,(0\,|\,0)$, the EKF enters a loop that alternates between prediction and correction steps.

During the prediction phase, the algorithm computes the predicted state vector $\hat{x}\,(k+1\,|\,k)$ and the covariance matrix of prediction errors $\mathbf{P}\,(k+1\,|\,k)$. Before performing these computations, the continuous dynamics model (15) is linearized. Specifically, the fundamental matrix $\mathbf{F} = \left.\dfrac{\partial \mathbf{f}(\mathbf{x})}{\partial \mathbf{x}}\right|_{\mathbf{x}=\hat{x}}$ is calculated as the Jacobian of the nonlinear function $\mathbf{f}(\mathbf{x})$. Using $\mathbf{F}$ and the disturbance input matrix $\mathbf{G}$ from (15), the continuous model is then sampled to obtain its discrete counterpart. This sampling, as described in [12], yields the transition matrix $\mathbf{\Phi}$ and the matrix of discrete process disturbances $\mathbf{Q}$, both of which are essential for the prediction step.

In the correction phase (illustrated in the final block of the loop in Fig. 3), the following are computed: the Kalman gain matrix $\mathbf{K}$, the updated (filtered) state vector $\hat{x}\,(k+1 \mid k+1)$ and the updated covariance matrix of filtering errors $\mathbf{P}\,(k+1 \mid k+1)$. This step requires linearizing the observation model (23) to obtain the observation matrix $\mathbf{H} = \left.\dfrac{\partial \mathbf{h}\,(\mathbf{x})}{\partial \mathbf{x}}\right|_{\mathbf{x}=\hat{x}}$, which is the Jacobian of the nonlinear function $\mathbf{h}\,(\mathbf{x})$. In addition, the covariance matrix of measurement errors $\mathbf{R}$ must be computed. This is accomplished by $\mathbf{R} = \mathbf{T}\mathbf{R}'\mathbf{T}^T$, where $\mathbf{T}$ is the Jacobian matrix of the transformation function $\mathbf{t}\,(\cdot)$, and $\mathbf{R}'$ is the covariance matrix of the primary measurement errors (containing the variances of the azimuth and elevation angles from the primary measurement vector $\mathbf{z}'$).

The OLS and WLS algorithms are described in detail in [19]. These algorithms iteratively solve the nonlinear observation model (23) to determine the ballistic object's position. However, as they do not incorporate the dynamics model or utilize predicted state estimates from the previous steps, their estimates are neither as accurate nor as smooth as those produced by the EKF. Furthermore, while OLS and WLS are limited to estimating only the object's position, the EKF proposed in this research also estimates several additional flight parameters, including the object's velocity v, attitude angles γ and χ, mass m, and wind velocity components. These additional estimates are particularly valuable, as they enable more accurate predictions of the ballistic target's impact site [20].

3. Experiments and results

The electro-optical tracking system (EOTS) and the ballistic object were modelled and simulated in MATLAB®. Figure 4 presents a typical shooting test layout that shows the positions of two cinetheodolites and a simulated trajectory of the ballistic object. The figure displays both the actual trajectory (labelled "REF") and the trajectories estimated using various algorithms (OLS, WLS, and EKF). In these simulations, the ballistic object's parameters were assumed to be identical to those of the aerial target imitator ICP-89 [17]. The angular measurement accuracy (for both azimuths and elevations) was taken from the system specifications, with standard deviations of 0.68 arcsec.

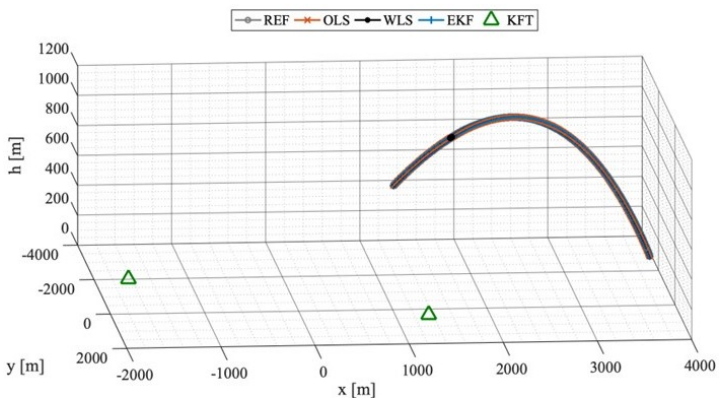

Fig. 4. Reference and estimated trajectories of the ballistic object.

Figures 5–7 illustrate the position coordinates estimation errors for the various algorithms. As shown, the accuracies of OLS and WLS are similar, while the proposed EKF delivers noticeably better performance. Additionally, Figures 8–13 present estimates of other flight parameters and wind velocities, which are available only through the EKF. These estimates closely match the actual parameter values, further demonstrating the high performance of the proposed EKF algorithm.

Metrol. Meas. Syst., Vol. 32 (2025), No. 2, pp. 1–14
DOI: 10.24425/mms.2023.154667

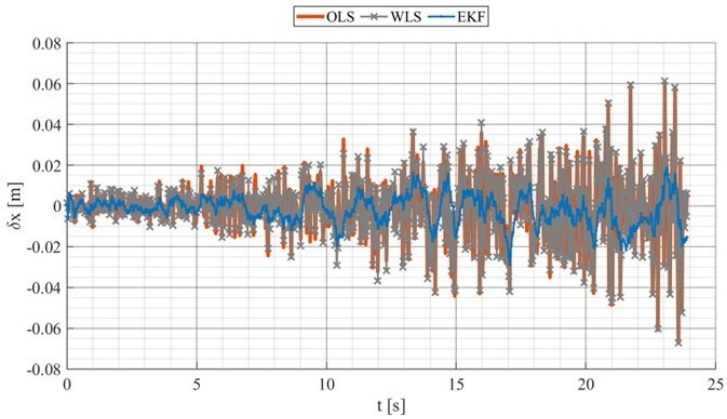

Fig. 5. Estimation errors for the x coordinate.

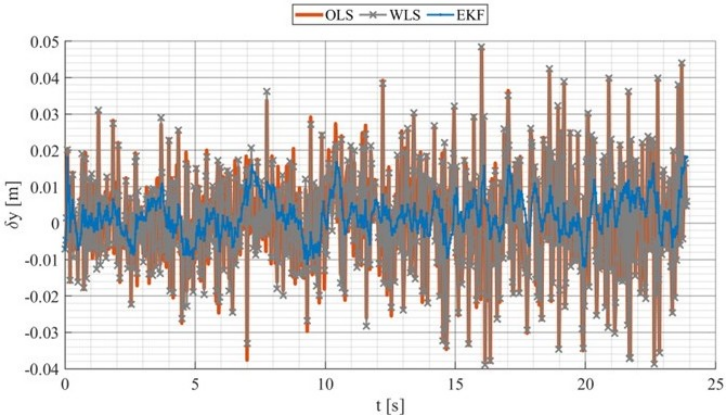

Fig. 6. Estimation errors for the y coordinate.

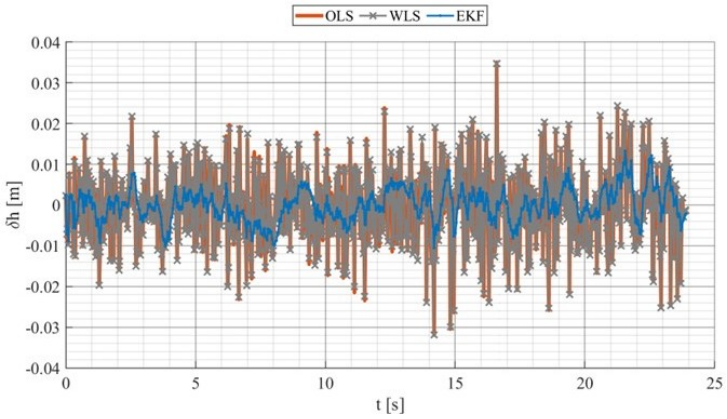

Fig. 7. Estimation errors for altitude h.

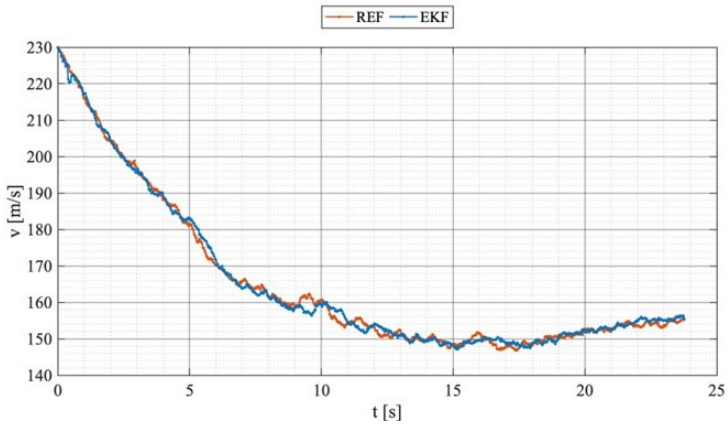

Fig. 8. Reference and estimated velocity of the ballistic object.

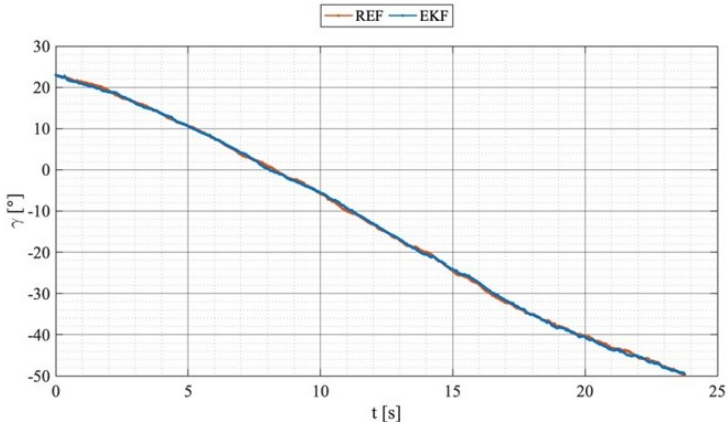

Fig. 9. Reference and estimated γ angle of the ballistic object.

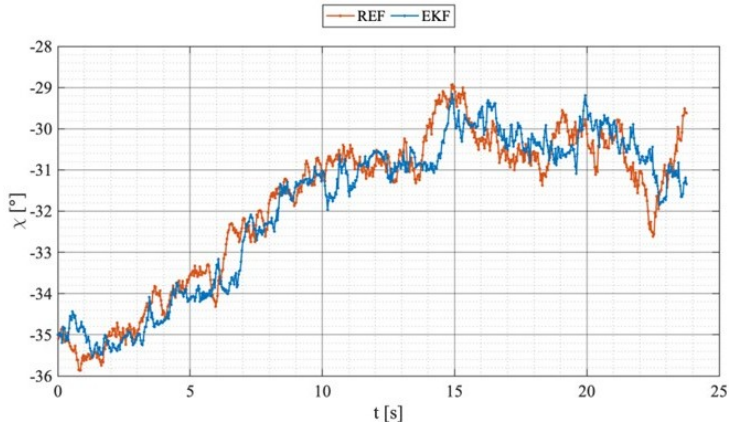

Fig. 10. Reference and estimated χ angle of the ballistic object.

Metrol. Meas. Syst., Vol. 32 (2025), No. 2, pp. 1–14
DOI: 10.24425/mms.2023.154667

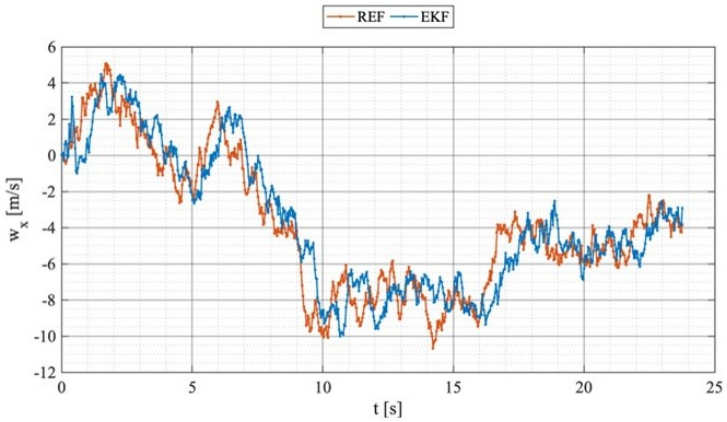

Fig. 11. Reference and estimated w_x component of wind velocity.

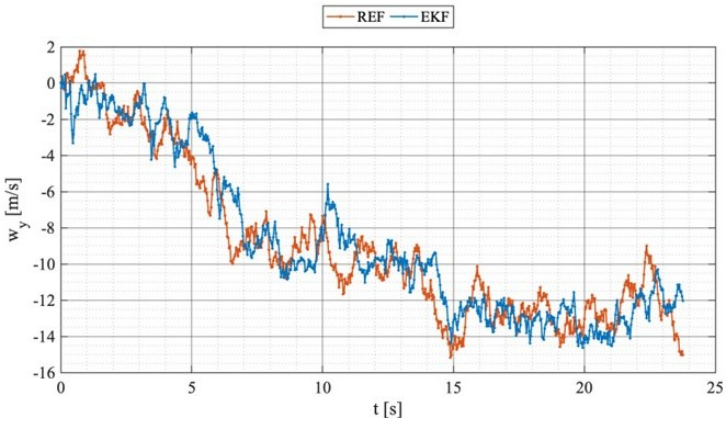

Fig. 12. Reference and estimated w_y component of wind velocity.

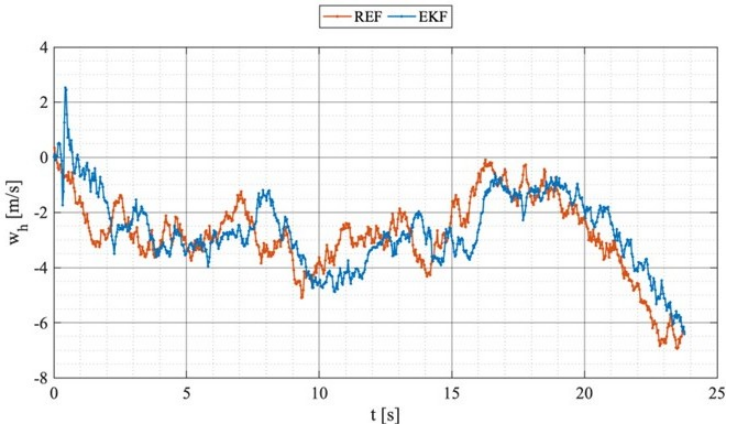

Fig. 13. Reference and estimated w_h component of wind velocity.

To quantitatively evaluate the position estimation accuracy of the considered algorithms (OLS, WLS, and EKF), the simulations were repeated 1,000 times, and the root-mean-squared (RMS) errors for all coordinates were computed [21]. These results are presented in Table 1 for various flight durations (after 1, 8, 15, and 20 seconds) as well as for the entire trajectory. The final two columns of the table compare the EKF's positioning errors with those of OLS and WLS, demonstrating a significant improvement in accuracy over these simpler algorithms.

As demonstrated in Table 1, the position estimation errors obtained with all methods (OLS, WLS, and EKF) increase monotonically at selected time points during the flight, which is expected because identical angular measurement errors yield larger position errors as the ballistic object moves further from the cinetheodolites. This is a consequence of the tracking system's geometry and is observed in various optical and radar systems that rely on angle measurements for position estimation. Consequently, increasing errors during the final phase of the flight are also evident in the estimates of other quantities, as shown in Figs. 4–13. This should not be interpreted as a deficiency of the developed EKF algorithm or the other methods. The increase in estimation errors is relatively small and can be mitigated by optimally positioning the cinetheodolites relative to the anticipated flight trajectory or by increasing their number in the system.

Table 1. Comparison of OLS, WLS and EKF estimation errors.

Error	**OLS**	**WLS**	**EKF**	**Improvement ratio**	
				$\frac{\text{EKF}}{\text{OLS}}$	$\frac{\text{EKF}}{\text{WLS}}$
RMS δx_1 $[m]$	$0.42 \cdot 10^{-2}$	$0.40 \cdot 10^{-2}$	$0.24 \cdot 10^{-2}$	1.72	1.65
RMS δx_8 $[m]$	$1.00 \cdot 10^{-2}$	$0.92 \cdot 10^{-2}$	$0.47 \cdot 10^{-2}$	2.11	1.94
RMS δx_{15} $[m]$	$1.70 \cdot 10^{-2}$	$1.66 \cdot 10^{-2}$	$0.80 \cdot 10^{-2}$	2.13	2.09
RMS δx_{20} $[m]$	$2.40 \cdot 10^{-2}$	$2.38 \cdot 10^{-2}$	$1.02 \cdot 10^{-2}$	2.35	2.33
RMS δx $[m]$	$1.57 \cdot 10^{-2}$	$1.55 \cdot 10^{-2}$	$0.70 \cdot 10^{-2}$	2.26	2.22
RMS δy_1 $[m]$	$0.89 \cdot 10^{-2}$	$0.89 \cdot 10^{-2}$	$0.48 \cdot 10^{-2}$	1.86	1.85
RMS δy_8 $[m]$	$1.22 \cdot 10^{-2}$	$1.20 \cdot 10^{-2}$	$0.55 \cdot 10^{-2}$	2.21	2.17
RMS δy_{15} $[m]$	$1.65 \cdot 10^{-2}$	$1.64 \cdot 10^{-2}$	$0.75 \cdot 10^{-2}$	2.20	2.19
RMS δy_{20} $[m]$	$1.98 \cdot 10^{-2}$	$1.99 \cdot 10^{-2}$	$0.91 \cdot 10^{-2}$	2.17	2.17
RMS δy $[m]$	$1.49 \cdot 10^{-2}$	$1.48 \cdot 10^{-2}$	$0.69 \cdot 10^{-2}$	2.15	2.14
RMS δh_1 $[m]$	$0.70 \cdot 10^{-2}$	$0.70 \cdot 10^{-2}$	$0.37 \cdot 10^{-2}$	1.91	1.91
RMS δh_8 $[m]$	$0.95 \cdot 10^{-2}$	$0.94 \cdot 10^{-2}$	$0.40 \cdot 10^{-2}$	2.38	2.36
RMS δh_{15} $[m]$	$1.04 \cdot 10^{-2}$	$1.04 \cdot 10^{-2}$	$0.44 \cdot 10^{-2}$	2.37	2.36
RMS δh_{20} $[m]$	$1.01 \cdot 10^{-2}$	$1.01 \cdot 10^{-2}$	$0.46 \cdot 10^{-2}$	2.19	2.19
RMS δh $[m]$	$0.95 \cdot 10^{-2}$	$0.95 \cdot 10^{-2}$	$0.42 \cdot 10^{-2}$	2.25	2.25

4. Conclusions

The estimation algorithm for tracking aerial ballistic objects, such as unguided short-range missiles, presented in this paper, demonstrates high performance when using measurements from an electro-optical tracking system. By applying a 6-DOF object movement model, the algorithm enables the estimation of the object's three-dimensional position within a geographically oriented

horizontal frame of reference, without requiring prior knowledge of the shooting direction. This makes the algorithm simple in practical implementation, as determining this direction before the missile is launched might be problematic.

In terms of RMS errors for the x, y, and h position coordinates, the estimation errors are reduced by approximately a factor of two or more compared to the OLS and WLS methods. Additionally, the proposed filtration algorithm allows for the direct estimation of movement parameters that are not directly measurable by the electro-optical tracking system, such as the magnitude and direction of the velocity vector, represented by the angles γ and χ between this vector and the $EXYZ$ coordinate system axes. Furthermore, by incorporating the proposed dynamics model in the extended Kalman filter, additional important information can be obtained, including the three-dimensional wind velocity components.

The high accuracy of the estimated data demonstrates the algorithm's potential for real-world applications. One possible application is more accurate and confident estimation of an object's impact location, outperforming traditional methods. Another practical use would be in calculating the miss distance during homing missile tests.

Acknowledgements

This work was supported by the Military University of Technology, Poland, under research project UGB/22-056/2025/WAT.

References

[1] Smagowski, P. (2020). *Estymacja parametrów lotu niekierowanego pocisku rakietowego z wykorzystaniem optoelektronicznego systemu trajektograficznego*. [Doctoral dissertation, Wojskowa Akademia Techniczna]. https://bip.wat.edu.pl/bip/dokumenty/postepowania-awansowe/psmagowski/rozprawa_doktorska_piotr_smagowski.pdf

[2] Kaniewski, P., Smagowski, P., & Konatowski, S. (2019). Ballistic Target Tracking with Use of Cinetheodolites. *International Journal of Aerospace Engineering*, *2019*, 1–13. https://doi.org/10.1155/2019/3240898

[3] Kim, J. (2023b). Computationally efficient Ground-to-Air missile seeker based on camera images. *IEEE Access*, *11*, 104839–104845. https://doi.org/10.1109/access.2023.3318745

[4] Moon, K., Kwon, H., Ryoo, C., & Sim, H. (2018). Trajectory estimation for a ballistic missile in ballistic phase using IR images. In *Proceedings of the 9th International Conference on Mechanical and Aerospace Engineering (ICMAE)* (pp. 173–177). https://doi.org/10.1109/icmae.2018.8467635

[5] Słowak, P., & Kaniewski, P. (2023). Homography augmented particle filter SLAM. *Metrology and Measurement Systems*. https://doi.org/10.24425/mms.2023.146420

[6] Wang, X., & Li, C. (2021). Cooperative Tracking of Hypersonic Target with Bearing-Only Measurements. *Proceedings of the 40th Chinese Control Conference (CCC)* (pp. 5212–5216). https://doi.org/10.23919/ccc52363.2021.9549405

[7] Paś, J., Rosiński, A., & Białek, K. (2021). A reliability-operational analysis of a track-side CCTV cabinet taking into account interference. *Bulletin of the Polish Academy of Sciences. Technical Sciences*, 136747. https://doi.org/10.24425/bpasts.2021.136747

[8] Costa, P., & Moore, W. (2002). Extended Kalman-Bucy filters for radar tracking and identification. *Proceedings of the IEEE National Radar Conference*, 127–131. https://doi.org/10.1109/nrc.1991.114744

[9] Farina, A., Del Gaudio, M., D'Elia, U., Immediata, S., Ortenzi, L., Timmoneri, L., & Toma. (2004). Detection and tracking of ballistic target. *Proceedings of the IEEE National Radar Conference* (pp. 450–456). https://doi.org/10.1109/nrc.2004.1316467

[10] Aditya, P., Apriliani, E., Arif, D. K., & Baihaqi, K. (2018). Estimation of three-dimensional radar tracking using modified extended Kalman filter. *Journal of Physics Conference Series*, *974*, 012071. https://doi.org/10.1088/1742-6596/974/1/012071

[11] Abreu, J. a. P., Neto, J. V. F., & Oliveira, R. C. L. (2011). Ballistic Rockets tracking: Kalman versus $\alpha\beta\gamma$ filters. *Proceedings of the 13th International Conference on Modelling and Simulation (UKSim)* (pp. 313–318). https://doi.org/10.1109/uksim.2011.66

[12] Brown, R. G., & Hwang, P. Y. C. (1992). Introduction to random signals and applied Kalman filtering. In *John Wiley and Sons eBooks*. http://ci.nii.ac.jp/ncid/BA17030473

[13] Blackman, S. S., & Populi, R. (1999). *Design and Analysis of Modern Tracking Systems*. http://ci.nii.ac.jp/ncid/BA43213153

[14] Hull, D. G. (2007). Fundamentals of Airplane Flight Mechanics. In *Springer eBooks*. https://doi.org/10.1007/978-3-540-46573-7

[15] Siouris, G. M. (2004). Missile guidance and control systems. *Applied Mechanics Reviews*, *57*(6), B32. https://doi.org/10.1115/1.1849174

[16] Sahbon, N., & Welcer, M. (2024). Comparison of two aerodynamic models for projectile trajectory simulation. *Aerospace*, *11*(3), 189. https://doi.org/10.3390/aerospace11030189

[17] Świderski, W., Kaczmarzyk, J., & Szklarski, A. (2014). Wybrane zagadnienia projektowania kierowanego imitatora celu powietrznego ICP 12S6. *Problemy Techniki Uzbrojenia*. http://yadda.icm.edu.pl/baztech/element/bwmeta1.element.baztech-187b3033-ae97-4c81-8996-4851d352bcc1

[18] National Aeronautics and Space Administration. (1976). *U.S. Standard Atmosphere, 1976* (NASA-TM-X-74335). NASA Technical Reports Server. https://ntrs.nasa.gov/api/citations/19770009539/downloads/19770009539.pdf

[19] Kailath, T., Sayed, A. H., & Hassibi, B. (2000). *Linear Estimation*. Prentice Hall.

[20] Zhang, X., Lei, H., Li, J., & Zhang, D. (2014). Ballistic missile trajectory prediction and the solution algorithms for impact point prediction. In *Proceedings of the 2014 IEEE Chinese Guidance, Navigation and Control Conference* (pp. 879–883). https://doi.org/10.1109/cgncc.2014.7007325

[21] Lewicka, O. (2023). Method for accuracy assessment of topo-bathymetric surface models based on geospatial data recorded by UAV and USV vehicles. *Metrology and Measurement Systems*, 461–480. https://doi.org/10.24425/mms.2023.146421

Piotr Smagowski received his M.Sc. in 2006 and Ph.D. in 2022. He is currently working as an Assistant Professor at the Faculty of Electronics, Photonics and Microsystems at the Wroclaw University of Science and Technology. His current research is related to scanning probe microscopy, with focus on methods for estimation of the probe dynamic parameters.

Piotr Kaniewski received his M.Sc. in 1994, Ph.D. in 1998, and was habilitated in 2011. Currently, he works as an Associate Professor at the Faculty of Electronics at the Military University of Technology. His research is focused on navigation systems for special purposes, such as supporting synthetic aperture radars and ground penetrating radars as well as distributed estimation algorithms for UAV swarms, and navigation systems for GNSS denied environments. He has authored more than 200 scientific papers and 2 books.